 CMES, vol.23, no.1, pp.13-28, 2008

Analysis of EDL Effect for Pressure-Driven 3D Developing Micro-Scale Flow

E. Y. K. Ng[1] and S. T. Tan[2]

Abstract: Microchannels have been recognized as a very effective chemical separation and heat transfer device. The electrical double layer (EDL) effect in a micro-scale flow is however anticipated to be critical. In this paper, Nernst-Planck model (NPM), is used to predict the ion concentration distribution as it is reported to be a more appropriate model for developing microchannel flow. The governing equations are discretised for developing rectangular microchannel flows in Cartesians coordinate. An additional body force source term that is relating to the electric potential, resulted from the EDL effect is introduced in the conventional z-axis momentum equation as a body force, thereby modifying the flow characteristics. A finite-volume scheme is developed to solve the set of partial differential equations.

The focus of this paper is on the documentation for the effect of aspect- ratio (AR), Schmidt Number (Sc) and Wall Electrical Potential ($\overline{\xi}_o$) on the performance of microchannel including the friction coefficient (fRe), entrance length (L_e) and Nusselt number (Nu).

Keyword: Developing Flow; Heat Transfer; Micro-scale; EDL; Pressure-driven; Nernst-Planck

Nomenclature

AR	aspect ratio, $W_c/(2L_c)$
C_p	specify heat capacity of the fluid ($\mathrm{JKg^{-1}K^{-1}}$)
D_h	microchannel hydraulic diameter (m)
D_f	diffusion coefficient of ions ($\mathrm{m^2s^{-1}}$)
e	charge of electron (C)
Ec	Eckert number, $\frac{W_{in}^2}{C_P q'' D_h}$
E_z	electric field strength in the x, y-plane ($\mathrm{Vm^{-1}}$)
F	force (N)
f	friction factor, $f = \frac{8\tau_w}{\rho_f W_{in}^2}$
fRe	friction coefficient, the product of friction factor and Reynolds number
H_c	microchannel height (m)
h_x	local heat transfer coefficient ($\mathrm{Wm^{-2}K^{-1}}$)
k_f	thermal conductivity of the fluid ($\mathrm{Jm^{-1}K^{-1}}$)
L_c	microchannel length (m)
L_e	nondimensional entrance length, is defined as the streamline direction distance where the change of nondimensional velocity, W less than 1%
n_o	ionic number concentration (M)
n^+	cations concentration (M)
n^-	anions concentration (M)
Nu_x	local Nusselt number, $\frac{h_x D_h}{k_f}$
Nu_{ave}	average Nusselt number, $\frac{D_h}{L}\int_0^{L/D_h} Nu_x dx$
Re	Reynolds number, $\frac{\rho_f W_{in} D_h}{\mu_f}$
P	local fluid pressure ($\mathrm{Nm^{-2}}$)
Pr	Prandlt number, $\frac{\mu_f}{\rho_f \alpha}$
q''	heat flux at hot wall ($\mathrm{Wm^2}$)
Sc	Schmidt number, $Sc = \frac{\mu_f}{\rho_f D_f}$
Sc^+	Schmidt number of cation
Sc^-	Schmidt number of anion
T	Temperature (K)
U	channel mainstream velocity

[1] Corresponding author. School of Mechanical and Aerospace Engineering, College of Engineering, Nanyang Technological University, 50 Nanyang Avenue Singapore 639798. email: mykng@ntu.edu.sg, Tel: (065)6790-4455, Fax: (065)6791-1859

[2] Design Assurance, Seagate Technology International, 7000 Ang Mo Kio, Avenue 5, Singapore 569877.

	(ms^{-1})
W_c	microchannel width (m)
W_{in}	inlet velocity (ms^{-1})
X	x-direction coordinates (m)
Y	y-direction coordinates (m)
Z	z-direction coordinates (m)
z_i	valence of i type-ions
α	thermal diffusivity of the fluid (m^2s^{-1}), $\frac{k_f}{C_p\rho_f}$
ε	relative dielectric constant of the liquid
ε_o	dielectric constant of the liquid
λ	electric conductivity of ion $(\Omega^{-1}m)$
μ	dynamic viscosity of fluid $(Kgm^{-1}s^{-1})$
θ	dimensionless temperature
ρ	density (Kgm^{-3})
ρ_e	electrical charges per unit volume(Cm^{-3})
ρ_f	density of fluid (Kgm^{-3})
τ_w	wall shear stress (Nm^{-2})
ξ_0	wall electrical potential (V)
$\overline{\xi}_0$	nondimensional wall electrical potential, $\overline{\xi}_0 = \frac{z_i e \xi_o}{k_b T_{in}}$
Ψ	electric potential (V)

Superscript

$\bar{}$	nondimensional value
n	previous time step
n+1	current time step

Subscript

EDL	electric double layer
f	fluid properties
in	inlet
x	local value

1 Introduction

Microchannels have been identified with great potential in Micro-Electric-Mechanical Systems (MEMS) and many modern instrumental applications in chemical analysis and biomedical diagnostics. The common usage of microchannels that has been widely discussed includes cooling devices in electronic system by Tuckennan (1984). With the extreme large surface area to volume ratio, microchannels are suggested to be a good solution in solving the heat problem in an electronic device. Microchannels are also used by Fu et al. (2002) in the area of bioengineering; one of the important applications is in the separation of biological or chemical components, such as the separation of DNA in genetic engineering. It uses the principle of different mobility of dielectric particles to move in opposite direction of the electrical potential under an applied electric field. Zhong et al. (2002) examined the sheet-flow model for blood flow in capillaries in the pulmonary alveoli from micromechanical point of view.

However, different from larger scale channels, an extra body force due to electrical double layer (EDL) in microchannels is significant as reported by Mala et al. (1997), hence, affecting the flow and thermal performance of the microchannel as indicated by Friction coefficient, fRe and Nusselt number, Nu. Ng and Poh (2002) studied the flow and heat transfer characteristics of microchannels for developed 2D flow field, with different bulk ionic concentration, Zeta potential and the aspect ratio of the channel. Tardu (2004) investigated the EDL effect on the stability of planar channel flows, and estimated indirectly the resulting transitional Reynolds number. Most of the analysis for microchannels was however done in 2-D [Mala et al. (1997)]. When comparing to a 2-D model, a 3-D model is far more challenging to handle. A 3-D analysis is certainly important in order to obtain a more realistic prediction. One important aspect of a 3-D model was in demonstrating the effect of the aspect ratio, AR, with values far from zero or infinity. In a classical study [Shah and London (1978)], it was suggested that even for aspect ratio of 0.1, the performance of a rectangular channel such as the friction coefficient, fRe, is significantly different from that predicted using a 2-D model with AR = zero. In the application of separating the DNA, typical dimensions of microchannel [Fu et al. (2003)] were 39.95μm in depth and 80μm in width. In such cases, predictions using 2-D model would not be realistic. A recent study of full 3-D flow with EDL effect through a microchannel was reported in Tan and Ng (2003) to provide a better insight to the real flow field. Ng and Tan (2004, 2007) further presented the effects of the charge density

on the 3-D flow field including the developing region.

In some of the previous studies, Poisson-Boltzmann model (PBM) [Mala et al. (1997)] was applied with the assumption of Boltzmann's distribution of charge. PBM was being used most frequently in developed flow field, as it was simple and promising. However its suitability for developing flows is debatable [Yang et al. (2001)], as the assumption of Boltzmann equilibrium distributions remains a concern. Nernst-Planck model (NPM), on the other hand, represents a better model for developing flow, was proposed by Yang et al (2001) to investigate the 2-D velocity field of the microchannel in the developing region to represent a better model.

In this paper, the NPM is extended to temperature prediction for a 3-D flow field to allow a better insight into the real flow field. The studies are focus on the effect of several important parameters such as aspect ratio, AR, wall electrical potential, $\overline{\xi}_o$, and Schmidt number, Sc.

2 Numerical Model

A simple rectangular channel as shown in Fig. 1 is used as the current physical model. The coordinate system is set such that the X, Y, Z directions depict the width W_c, length L_c, and height H_c of the rectangular respectively. The main stream flow is along the z-direction. The origin is placed at the mid-width of the rectangular and this permits computation to be done on half of the model with a physical mesh (Fig. 2).

2.1 *Formulating of Surface Electrostatic Potential*

In micro scale flows, the effect of the EDL near the solid/liquid interface on liquid flow through a rectangular microchannel is significant and cannot be ignored. According to the theory of electrostatics, the relationship of the electrical potential, Ψ and the net charge density per unit volume, ρ_e at any position is given by the Poisson's equation:

$$\frac{\partial^2\Psi}{\partial X^2}+\frac{\partial^2\Psi}{\partial Y^2}+\frac{\partial^2\Psi}{\partial Z^2}=-\frac{\rho_e}{\varepsilon\varepsilon_o} \tag{1}$$

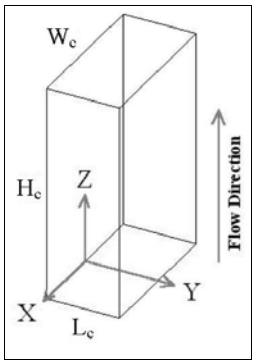

Figure 1: Physical model of the research (not in scale).

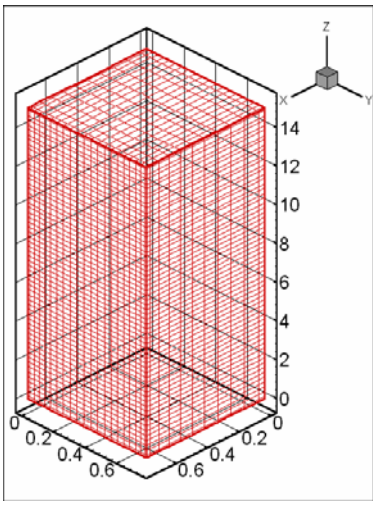

Figure 2: Mesh for the computation (not in scale).

where ε is the dielectric constant of the medium and ε_o is the electric permittivity of a vacuum.

Using the following nondimensional term:

$$x=\frac{X}{D_h} \quad y=\frac{Y}{D_h} \quad z=\frac{Z}{D_h} \quad \psi=\frac{z_1 e\Psi}{k_b T}$$

and

$$D_h=\frac{4L_cW_c}{2(L_c+W_c)}$$

where x is the nondimensional X-coordinate, y is the nondimensional Y-coordinate; z is the nondimensional Z-coordinate, D_h is the hydraulic diameter of the channel and ψ is the nondimensional electrostatic potential. The nondimensional form

of the 3-D Poisson's equation can be rewritten as:

$$\frac{\partial^2\psi}{\partial x^2}+\frac{\partial^2\psi}{\partial y^2}+\frac{\partial^2\psi}{\partial z^2}=-\frac{\rho_e}{2n_oz_1e}\frac{2n_oz_i^2e^2D_h^2}{\varepsilon\varepsilon k_bT} \quad (2)$$

where, $z_i$is valence of ions, $k_b$is Boltzmann's constant (1.3805×10^{-23} Jmol^{-1}K^{-1}), $T_{in}$is absolute temperature of fluid at inlet of microchannel (K), e is electron charge (1.6021×10^{-19} C), $n_o$is bulk concentration of ions.

As the net volume charge density ρ_e is proportional to the concentration difference between cations and anions, we have:

$$\rho_e=(n^+-n^-)z_ie \quad (3)$$

where n^+ and n^- are concentration of cations and anions respectively.

Hence

$$\frac{\partial^2\psi}{\partial x^2}+\frac{\partial^2\psi}{\partial y^2}+\frac{\partial^2\psi}{\partial z^2}=-K^2\frac{(n^+-n^-)}{2n_o} \quad (4)$$

where

$$K=D_h\kappa \quad (5)$$

$$\kappa=\left(\frac{2n_oz^2e^2}{\varepsilon\varepsilon k_bT}\right)^{\frac{1}{2}} \quad (6)$$

is Debye-Huckel parameter ($1/\kappa$ is normally referred as the EDL thickness).

Two Poisson equations termed after NP [Fu et al. (2003)] are applied to model the distribution of the concentration of charge particle (cations,n^+ and anions, n^-), based on the conservation law for cations and anions,

$$\frac{\partial\left(u\overline{n^+}\right)}{\partial x}+\frac{\partial\left(v\overline{n^+}\right)}{\partial y}+\frac{\partial\left(w\overline{n^+}\right)}{\partial z}=\frac{1}{Sc^+Re}\left(\frac{\partial^2\overline{n^+}}{\partial x^2}+\frac{\partial^2\overline{n^+}}{\partial y^2}+\frac{\partial^2\overline{n^+}}{\partial z^2}\right)+\frac{1}{Sc^+Re}\cdot\left[\frac{\partial}{\partial x}\left(\overline{n^+}\frac{\partial\psi}{\partial x}\right)+\frac{\partial}{\partial y}\left(\overline{n^+}\frac{\partial\psi}{\partial y}\right)+\frac{\partial}{\partial z}\left(\overline{n^+}\frac{\partial\psi}{\partial z}\right)\right] \quad (7)$$

$$\frac{\partial\left(u\overline{n^-}\right)}{\partial x}+\frac{\partial\left(v\overline{n^-}\right)}{\partial y}+\frac{\partial\left(w\overline{n^-}\right)}{\partial z}=\frac{1}{Sc^-Re}\left(\frac{\partial^2\overline{n^-}}{\partial x^2}+\frac{\partial^2\overline{n^-}}{\partial y^2}+\frac{\partial^2\overline{n^-}}{\partial z^2}\right)-\frac{1}{Sc^-Re}\cdot\left[\frac{\partial}{\partial x}\left(\overline{n^-}\frac{\partial\psi}{\partial x}\right)+\frac{\partial}{\partial y}\left(\overline{n^-}\frac{\partial\psi}{\partial y}\right)+\frac{\partial}{\partial z}\left(\overline{n^-}\frac{\partial\psi}{\partial z}\right)\right] \quad (8)$$

where Re is $(\frac{\rho_fW_{in}D_h}{\mu_f})$ Reynolds number and Schmidt number is defined as $Sc=\frac{\mu_f}{\rho_fD_f}$. $\overline{n^+}$, $\overline{n^-}$ is dimensionless cations and anion concentration, $\overline{n^+}=\frac{n^+}{n_o}$, $\overline{n^-}=\frac{n^-}{n_o}$. D_f is diffusion coefficient of ions (m^{2}s^{-1}).

As the physical model is symmetric, only one half of the rectangular microchannel is considered for the computational domain and depicted in Fig. 2.

The boundary conditions applicable to the electrostatic potential distribution are as follows:

At the wall of the microchannel ($x=W_c/2D_h$, $y=0$ and $y=L_c/D_h$), $\psi=\overline{\xi}_o$, $\overline{n^+}=e^{-\overline{\xi}_o}$ and $\overline{n^-}=e^{\overline{\xi}_o}$.

At symmetry boundary condition ($x=0$), $\frac{d\psi}{dx}=0$, $\frac{d\overline{n^+}}{dx}=0$ and $\frac{d\overline{n^-}}{dx}=0$.

At the inlet, where ($z=0$), $\psi=0$, $\overline{n^+}=1$ and $\overline{n^-}=1$,

At the outlet, where ($z=H_c/D_h$), $\frac{d\psi}{dz}=0$, $\frac{d\overline{n^+}}{dz}=0$ and $\frac{d\overline{n^-}}{dz}=0$,

where

$$\overline{\xi}_0=\frac{z_1e\xi_o}{k_bT_{in}}$$

ξ_o is the Zeta potential on wall.

2.2 Inclusion of EDL Effect with Navier-Stokes Equations

An extra body force in Z-direction originating due to the presence of the EDL is considered so as to modify the conventional Navier-Stokes equation [Mala et al. (1997)]. Therefore, the Navier-Stokes equations of 3-D steady state developing flow for microchannel are given as:

Continuity Equation

$$\frac{\partial u}{\partial x}+\frac{\partial v}{\partial y}+\frac{\partial w}{\partial z}=0 \quad (9)$$

Momentum Equations

x-direction

$$u\frac{\partial u}{\partial x}+v\frac{\partial u}{\partial y}+w\frac{\partial u}{\partial z}=\frac{1}{Re}\left(\frac{\partial^2u}{\partial x^2}+\frac{\partial^2u}{\partial y^2}+\frac{\partial^2u}{\partial z^2}\right)-\frac{\partial p}{\partial x} \quad (10)$$

y-direction

$$u\frac{\partial v}{\partial x}+v\frac{\partial v}{\partial y}+w\frac{\partial v}{\partial z} = \frac{1}{Re}\left(\frac{\partial^2 v}{\partial x^2}+\frac{\partial^2 v}{\partial y^2}+\frac{\partial^2 v}{\partial z^2}\right)-\frac{\partial p}{\partial y} \quad (11)$$

z-direction

$$u\frac{\partial w}{\partial x}+v\frac{\partial w}{\partial y}+w\frac{\partial w}{\partial z} = \frac{1}{Re}\left(\frac{\partial^2 w}{\partial x^2}+\frac{\partial^2 w}{\partial y^2}+\frac{\partial^2 w}{\partial z^2}\right)-\frac{\partial p}{\partial z}-\overline{G}_1\overline{E}_z\overline{\rho}_e \quad (12)$$

Energy Equation

$$u\frac{\partial \theta}{\partial x}+v\frac{\partial \theta}{\partial y}+w\frac{\partial \theta}{\partial z}=\frac{1}{Re}\left(\frac{\partial^2 \theta}{\partial x^2}+\frac{\partial^2 \theta}{\partial y^2}+\frac{\partial^2 \theta}{\partial z^2}\right) + \frac{Ec}{Re}\left\{2\left[\left(\frac{\partial u}{\partial x}\right)^2+\left(\frac{\partial v}{\partial y}\right)^2+\left(\frac{\partial w}{\partial z}\right)^2\right] + \left[\frac{\partial u}{\partial y}+\frac{\partial v}{\partial x}\right]^2+\left[\frac{\partial w}{\partial y}+\frac{\partial v}{\partial z}\right]^2+\left[\frac{\partial u}{\partial z}+\frac{\partial w}{\partial x}\right]^2\right\} \quad (13)$$

The following dimensionless terms (all the undefined symbols are defined in the Nomenclature) are used.

$$u=\frac{U}{W_{in}},\quad v=\frac{V}{W_{in}},\quad w=\frac{W}{W_{in}},\quad p=\frac{P-P_{in}}{\rho_f W_{in}^2},$$

$$\theta=\frac{T-T_{in}}{q^{"}D_h},\quad \alpha=\frac{k_f}{C_p\rho_f},\quad Re=\frac{\rho_f W_{in}D_h}{\mu_f},$$

$$\mathrm{Pr}=\frac{\mu_f}{\rho_f\alpha},\quad Ec=\frac{W_{in}^2}{C_P q'' D_h},$$

$$\overline{G}_1=\frac{2n_o z_1 e\xi_o}{\rho W_{in}^2},\quad \overline{G}_2=\frac{2n_o z_1 e D_h W_{in}}{\lambda\xi_o}$$

$$\overline{E_z}=\left(\frac{D_h}{W_h}\right)\left(\frac{D_h}{L_h}\right)\overline{G_2} \cdot\frac{\int\left[\rho_e w-\left(eD_f\frac{\partial n^+}{\partial z}-eD_f\frac{\partial n^-}{\partial z}\right)\right]dA}{\int(\lambda n^+ +\lambda n^-)\,dA} \quad (14)$$

$$\overline{\rho}_e=\frac{(n^+-n^-)}{2n_o} \quad (15)$$

where λ is electric conductivity of ion (Ω^{-1}m). q'' is heat flux at hot wall (Wm^2). C_p is the specify heat capacity of the fluid (JKg^{-1}K^{-1}). k_f is the thermal conductivity of the fluid (Jm^{-1}K^{-1}).

The following boundary conditions are then applied to equations (9) to (13).

At the inlet of the channel, where $z=0$, the fluid is assumed to be uniform with $u=0$, $v=0$, $w=1$ and $\theta=0$.

At the outlet of the microchannel, where $z=H_c/D_h$, the flow is assumed to be fully developed in all of the velocity components and temperature (with $H_c=10\times W_c=20\times L_c$). Hence, the boundary conditions of $\frac{\partial u}{\partial z}=0$, $\frac{\partial v}{\partial z}=0$, $\frac{\partial w}{\partial z}=0$ and $\frac{\partial \theta}{\partial z}=0$ are applied.

For the two cold walls of the channel, where $x=W_c/2D_h$ and $y=L_c/D_h$, adiabatic condition is applied. Therefore, $u=0$, $v=0$, $w=0$ and $\frac{\partial \theta}{\partial z}=0$ are applied.

For the hot wall, where $y=0$, a uniform heat flux of q'' is applied and electric potential on wall is ξ_o. Thus, $u=0$, $v=0$, $w=0$ and $\frac{d\theta}{dy}=\frac{q"D_h}{k}$ can be applied.

Finally, at the symmetric boundary, we have $x=0$, $\frac{du}{dx}=0$, $\frac{dv}{dx}=0$, $\frac{dw}{dx}=0$ and $\frac{d\theta}{dx}=0$.

In this study, a simple fluid flow model is used as shown in Fig. 2. The fluid can be any liquid containing ions, for example a dilute aqueous 1:1 potassium chloride (KCL) solution or normal water. The value of parameters used here is listed in Table 1. The Schmidt number (Sc) is 10^5, Reynolds number *(Re)* is 60, and Debye-Huckel parameter (κ) is 100, unless stated. The one half of computational model is based on 10×20×60 orthogonal mesh, as shown in Fig. 2.

Grid convergence test was conducted according to the Richardson Extrapolation (RE) method [Roache (1994)]. The (10×20×60) orthogonal mesh was taken as the reference 'normal' mesh. The sampling was done at same middle point of the x-y-z Cartesian co-ordinates in which its dimensionless velocity values were noted when the grid was coarsen. The magnitude of the RE error estimator of the normal grid solution for both tests is 0.0002%. The normal grid value of the grid convergence index is 0.0006%. The result

Table 1: Value of parameters used in the model

Model Parameters	Values	Fluid Properties	Values
Width, W_c	40μm	Density, ρ_f	997 Kg/m^3
Length, L_c	20μm	Viscosity, μ_f	8.55×10^4 (Ns)/m^2
Height, H_c	400μm	Thermal Conductivity, k_f	0.613 W/(mK)
Hydraulic diameter, D_h	25.67μm	Heat Capacity, C_p	4179 J/(KgK)
-	-	Schmidt No., Sc	10^5
-	-	Reynolds No., Re	60
-	-	Prandtl No., Pr	6.22
-	-	Eckert number No., Ec	6.03×10^{-5}

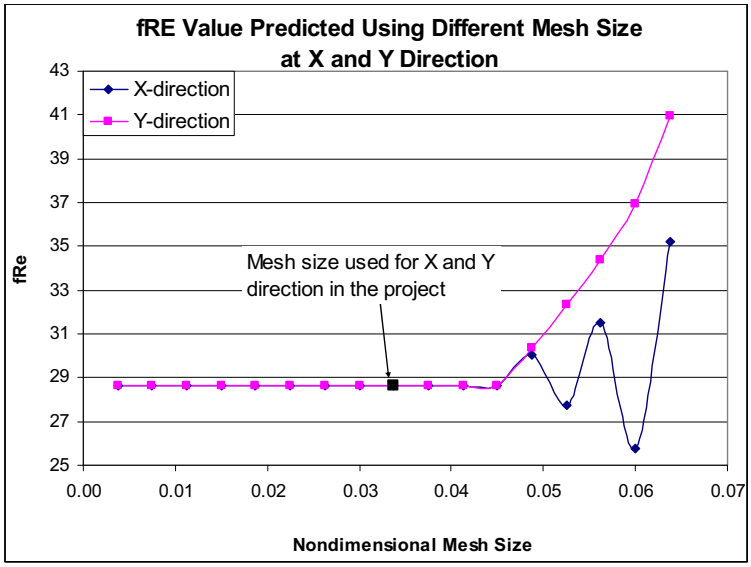

Figure 3: fRe values predicted using different mesh size at X and Y direction.

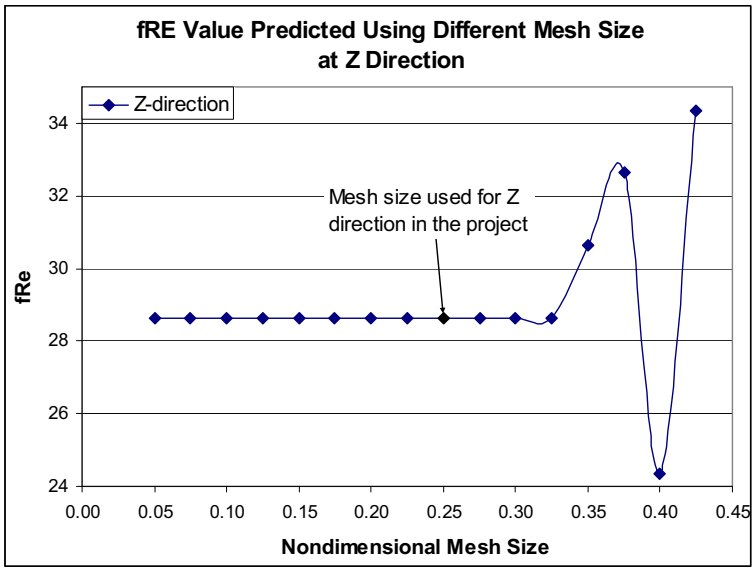

Figure 4: fRe values predicted using different mesh size at Z direction.

complied with the theory of RE error estimator, in which, E_1 is not conservative, whereas grid convergence index is conservative and quite so in the spirit of a 2-σ error band. For the grid sensitivity analysis, the two critical regions are the near wall region and the flow developing region, where important variables such as velocity, temperature and electrical potential change rapidly. The value of friction coefficient, fRe located at grid point (20, 40, 3) is used to check the robustness of the chosen mesh size. Fig. 3 and Fig. 4 show the predicted fRe value at grid point (20, 40, 3) for different mesh sizes. As shown in Fig. 3 the nondimensional mesh dimensions of 0.045 are sufficient to be used to predict accurate values in X and Y dimensions (i.e. grid invariance prediction). On the other hand, for Z dimension of the nondimensional mesh size, as shown in Fig. 4, it is found that a dimension of 0.25 is sufficient to predict the fRE value accurately.

The strongly non-linear governing equations (7-13) are solved using the finite volume numerical scheme based on Patankar (1980). The PDEs are first linearised using solution in general form with reasonable memory consumption and execution time, we then solve this linearised algebra problem in each non-linear iteration by nesting around the linear solver approach. Details of computational algorithm are documented in Ng and Tan (2004, 2007).

3 Results and Discussion

The effect of AR, Sc, $\overline{\xi}_o$ on the microchannel performance for 3D developing flow including including the fRe, L_e and Nu are studied and discussed next.

3.1 The Significant of Aspect Ratio (AR)

Compare to 2-D model, a 3-D model computation is far more challenging to handle and more CPU time is needed. However, for complex shapes and in cases where AR is not close to zero, a 3-D model is unavoidable. Effect of AR at developing region can only be studied using a 3-D model. In this section, a total of 5 AR values, 0.30, 0.50, 0.67, 0.75 and 1.00 are chosen to analyse the effect of aspect ratio for microchannels.

3.1.1 Friction coefficient, fRe

The fundamental different between micro and macro scale flow fields is the significant of the EDL effect. As the fluid contains ions flowing, counterion, which is attracted by the wall, will accumulate along the flow. Hence ions that accumulate at the down stream will build up an electrical field, which is the induced opposing electrical body force on the flow. As the EDL body force is an opposing force, it has similar effect with frictional force. Therefore it is expected the fRe value predicted with EDL effect is higher than that without EDL effect (see Table 2).

Fig. 5 shows the fRe value distribution along the z-direction (flow direction) for different AR values. It is found that the values of fRe increase with decreasing ARs. This can be explained as, the closer AR values to zero, the larger the relative surface area and hence the EDL effect is more significant.

Fig. 6 summarizes the fRe value in the fully developed region for the flow field predicted with and without EDL effects. The trend of the fRe value predicted with and without EDL effects is similar (Table 3). As the EDL body force is an opposing force; therefore it is found in Fig. 6 that the fRe values for flow field with EDL are generally higher than that without EDL effect.

3.1.2 Entrance length, L_e

For developing flow, the entrance length is one of important flow parameters. Fig. 7 shows the entrance length at different aspect ratio for both with and without EDL effects. The entrance length, Le, for prediction without EDL effect is based on the transitional empirical formula [Shah and London (1978)].

$$L_e \approx 0.06Re \tag{16}$$

and with the definition of Reynolds number, Re, equation (16) can be written as

$$L_e \approx 0.06\frac{\rho_f w D_h}{\mu_f} \tag{17}$$

Table 2: Compare the result predicted by NPM and the calculation without EDL effect

Predicted flow parameters	With EDL	No EDL
Friction Coefficient C_f or fRe at hot wall at fully developed region	16.8559	15.4233
Local Nusselt Nu_x at hot wall at fully developed region	3.730	4.137
Average Nusselt no. of the microchannel	4.410	4.891

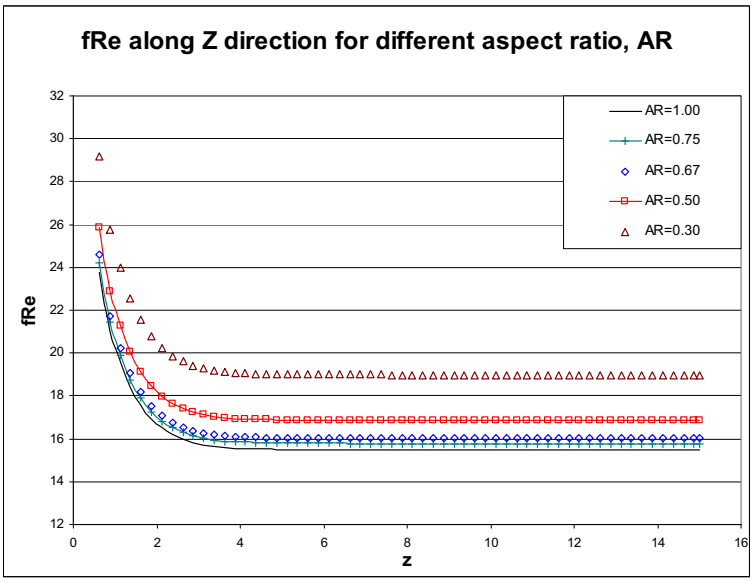

Figure 5: Friction Coefficient, fRe distribution along z-direction predicted with EDL effect for different aspect ratios, AR.

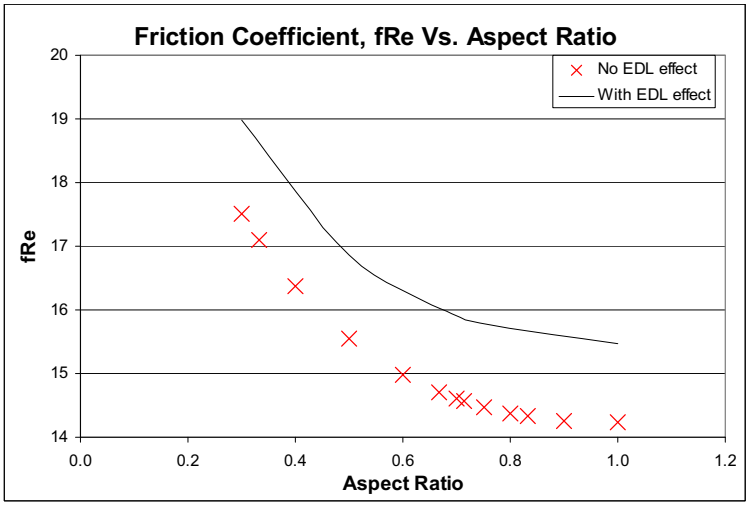

Figure 6: Friction coefficient, fRe, in the fully developed region for different aspect ratios, AR.

Table 3: Comparison of the percentage differences between fRe predicted with and without EDL effect at different aspect ratios

fRe value	AR = 0.3	AR = 0.5	AR = 1.0
with EDL Effect	18.99	16.86	15.48
Without EDL Effect	17.22	15.42	14.22
Percentage different	9.31%	8.52%	8.12%

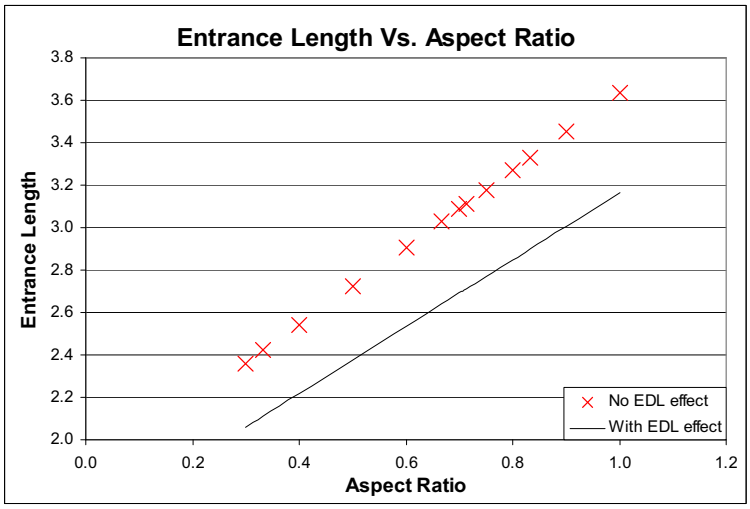

Figure 7: Entrance length for different aspect ratios, *AR*.

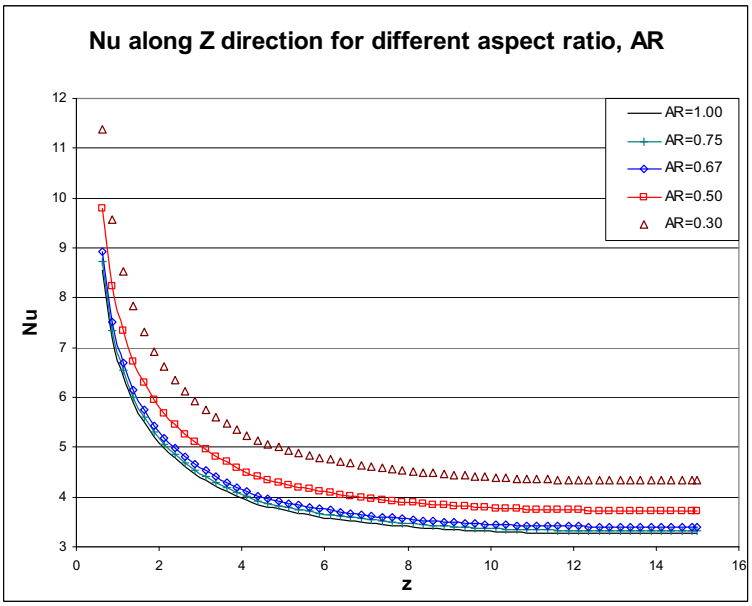

Figure 8: Nusselt Number, Nu distribution along z-direction for different aspect ratios, *AR*.

As shown in Fig. 7, with the higher effective viscous force due to the EDL effect, the flow field predicted with EDL effect is fully developed with a shorter entrance length. The results agree with equation (17), where L_e is inversely proportional to the viscosity.

3.1.3 Nusselt number, Nu

As shown in Fig. 8, the distribution of *Nu* values along the *z*-direction with various aspect ratios have similar trend to the distribution of fRe values. The *Nu* values decrease rapidly at the inlet region with steep gradient (as shown in Fig. 8). The *Nu* value for each *AR* reaches the fully developed region with a z-value of around 8. Fig. 9 summarizes the *Nu* values predicted by with and without EDL simulation in the fully developed region for different aspect ratios. It is found that the smaller aspect ratio produces higher *Nu* value. With the larger opposing force, extra heat is produced and hence reduces the effectiveness of heat transfer. Therefore, the *Nu* values with the EDL effect are lower than that without the EDL effect.

The *Nu* for a given *AR* approaches its asymptotic

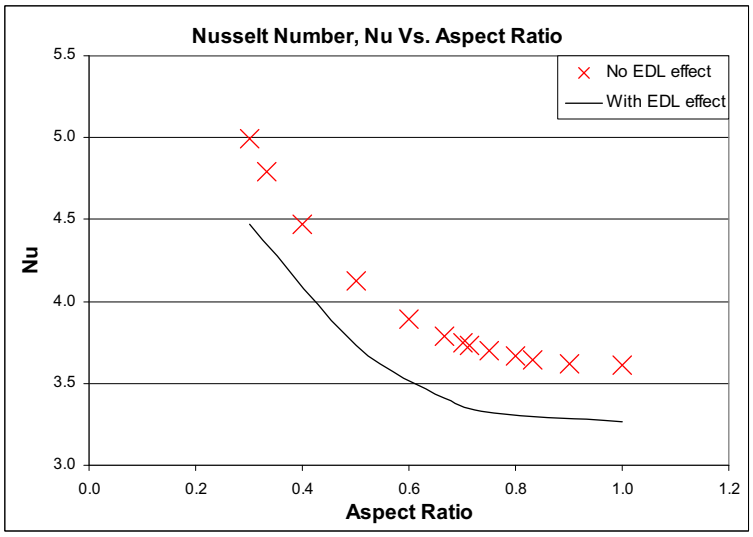

Figure 9: Nusselt number, Nu in the fully developed region for different aspect ratios, *AR*.

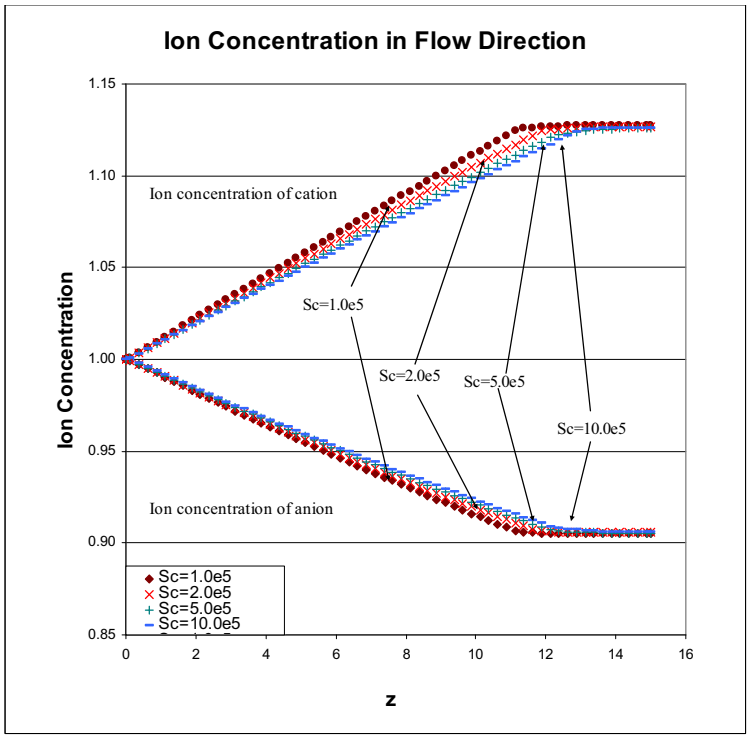

Figure 10: Cation and anion concentration distributions along z-direction at near wall grid.

value in the fully developed region for z greater than about 8.

Fig. 9 summarizes the variations of Nu values in the fully developed region for different aspect ratios. It is found that the smaller aspect ratio would result in higher Nu value. With the higher opposing force, extra heat is produced and hence reduces the efficiency of heat transfer. Therefore, the Nu values with EDL effect are lower than that without EDL effect. The percentage differences between Nu values predicted with and without EDL effect at different aspect ratios are summarized in Table 4.

In all, the discrepancy of fRe and Nu values for

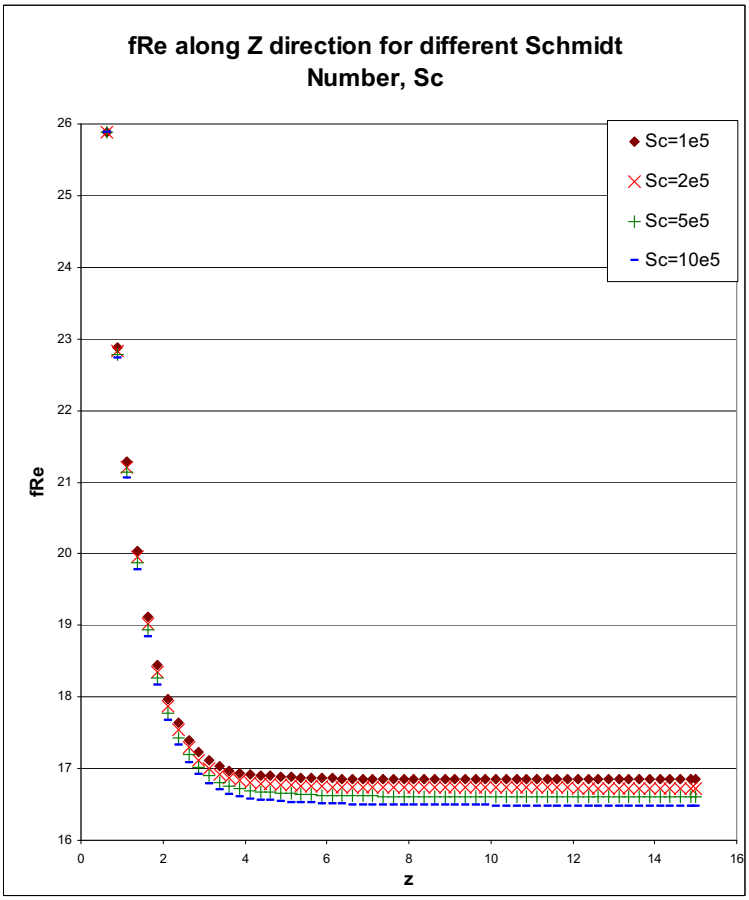

Figure 11: Friction coefficients, fRe distributions for different Schmidt numbers, *Sc*, on microchannel wall along the flow direction.

Table 4: Comparison of the percentage differences between *Nu* predicted with and without EDL effect at different aspect ratios

Nu value	AR = 0.3	AR = 0.5	AR = 1.0
with EDL Effect	4.474	3.730	3.264
without EDL Effect	4.962	4.137	3.620
Percentage different	-10.34%	-9.84%	-9.53%

different *AR* values are significant. As presented in Tables 3 and 4, in cases of the *ARs* equal to 0.3 and 1.0, the discrepancies of fRe and *Nu* can be up to 23% (18.99 for *AR*=0.3 and 15.48 for *AR*=1.0) and 37% (4.474 for *AR*=0.3 and 3.264 for *AR*=1.0) respectively for prediction with EDL effect. Therefore a 3-D analysis is concluded to be important and necessary for investigating the EDL effect in microchannel developing flow.

3.2 Comparing Results at Different Schmidt Numbers (Sc)

As compared to Poisson-Boltzmann model (an EDL model using Boltzmann distribution to describe ion concentration distribution), an extra parameter termed as $Sc = \frac{\mu_f}{\rho_f D_f}$, is found in the NPM (as shown in equations (7) and (8)). *Sc* represents the ratio of viscosity and diffusivity effects and thus is a function of fluid properties only. For a fixed Reynolds number, *Re*, the lower *Sc* value, the larger would be the diffusion layer. In this sec-

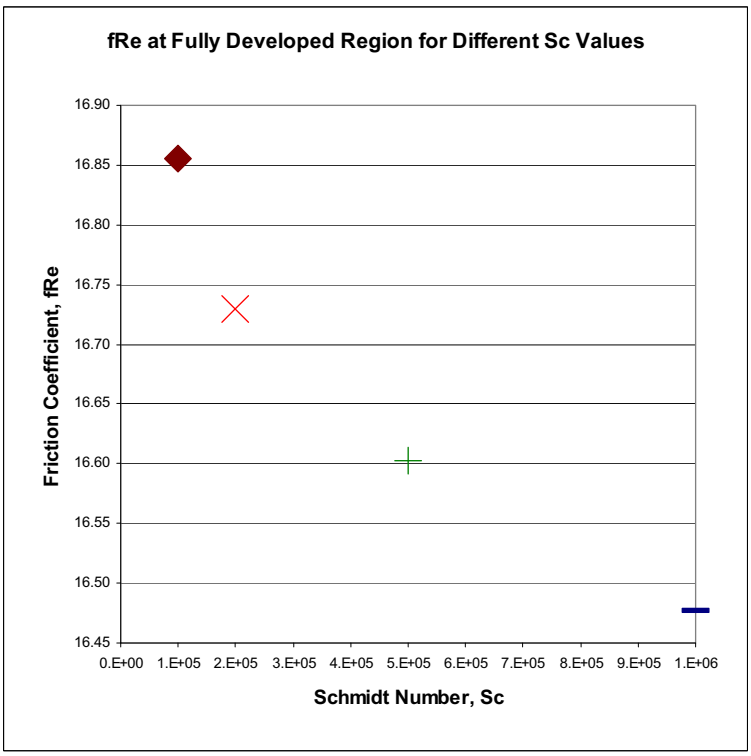

Figure 12: Friction coefficients, fRe in the fully developed region for different Schmidt numbers, Sc (♦:1e5, **x**:2e5, **+**:5e5, **-**:10e5).

tion, a total of 4 Sc values, 1e5, 2e5, 5e5 and 10e5 are chosen to analyse the effect of aspect ratio for microchannels.

As shown in Fig. 10, the anions concentration gradient, $\frac{\partial n^-}{\partial z}$ decreases as the Sc increases, but the cations concentration gradient $\frac{\partial n^+}{\partial z}$ increases. As a result, the value of $\left(\frac{\partial n^+}{\partial z} - \frac{\partial n^-}{\partial z}\right)$ increases and causes the EDL body force to reduce (since the $\left(\frac{\partial n^+}{\partial z} - \frac{\partial n^-}{\partial z}\right)$ is a positive term), which leads to a lower fRe as shown in Fig. 10.

The effect of Sc on fRe however is not so significant. Ten times increases in the Sc (1.0×10^5 to 1.0×10^6, see Fig. 12) only leads to 2% reduction in the fRe value (16.86 to 16.46). Note that the use of Sc $1.0\times10^6$is purely for investigative purpose since fluid with Sc 1.0×10^6may not be realistic.

3.3 *Effect of Wall Electric Potential,* $\overline{\xi}_o$

In this section, the effect of wall electrical potential $\overline{\xi}_o$ is studied. A total of five cases of dimensionless electrical potentials, $\overline{\xi}_o$ namely 1, 2, 3 and 4, are used as examples.

3.3.1 *Friction coefficient,* fRe

Fig. 13 shows the values of fRe at the near wall grids of the channel grid along the z-direction (streamwise), for $\overline{\xi}_o$=1, 2, 3 and 4. The plots are rather similar, and the flows become fully developed when z values are around 8. The deviation decreases when $\overline{\xi}_o$ is increased. As the applied wall electrical potential increases, the EDL effect increases and hence higher fRe.

Fig. 14 further shows an increase in the fRe with higher values of the wall electrical potential. The nondimensional fully developed velocities at the center of channel for $\overline{\xi}_o$ at 1 and 4 are 16.86 and 18.54 respectively. It is also observed that the difference in the nondimensional fully developed fRe is not linearly related with the wall electrical potential.

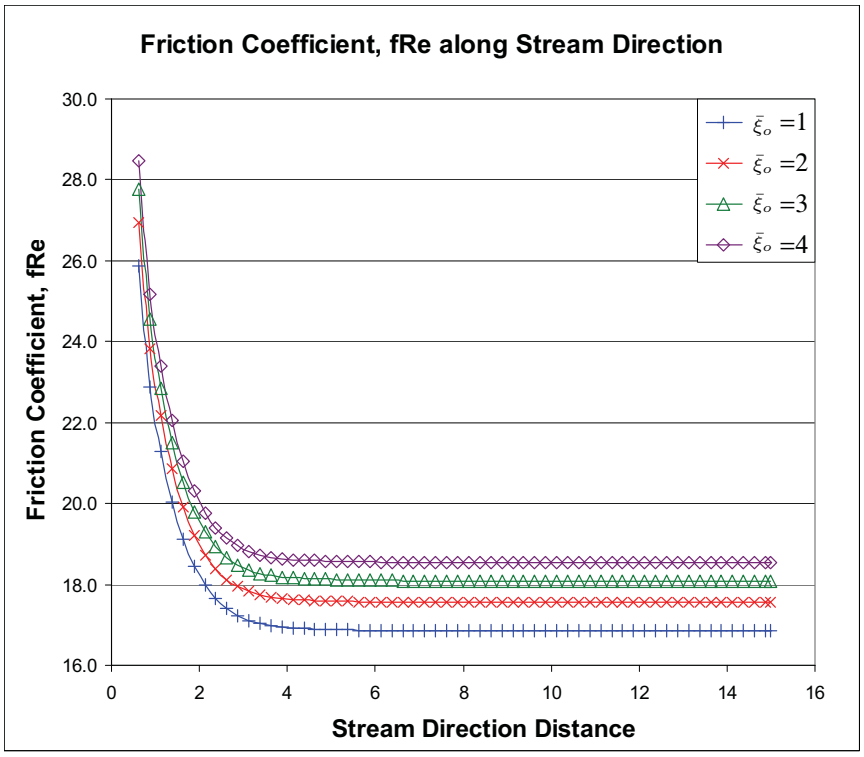

Figure 13: Friction coefficient along z-direction (streamwise).

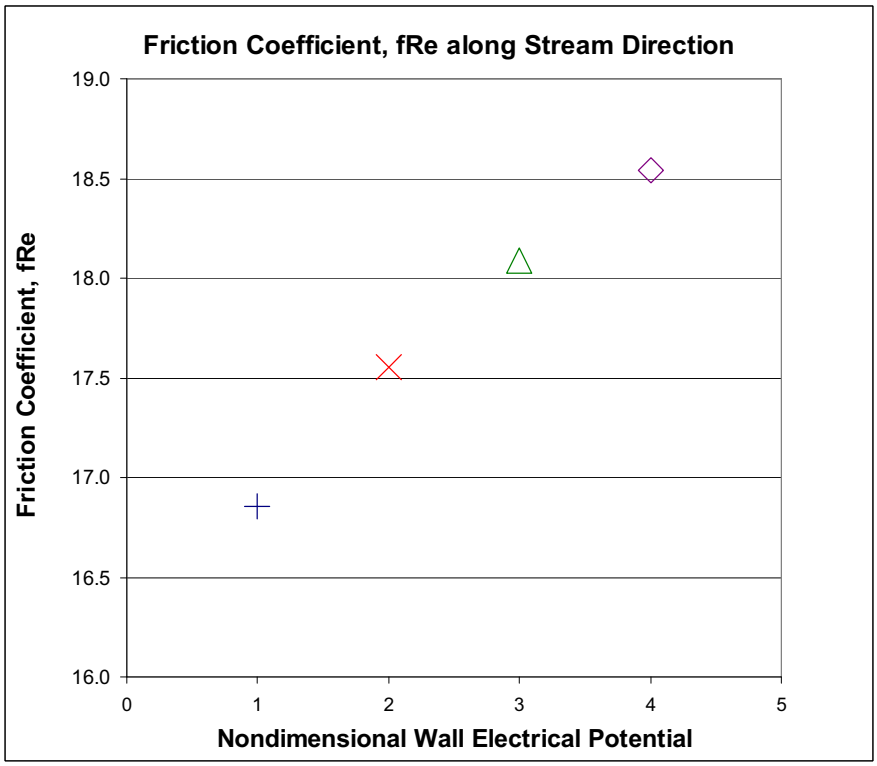

Figure 14: Friction coefficient vs. nondimensional wall electrical potential, $\overline{\xi}_0$, (◇:$\overline{\xi}_0$=1, Δ: $\overline{\xi}_0$=2, **x**: $\overline{\xi}_0$=3, **+**:$\overline{\xi}_0$=4).

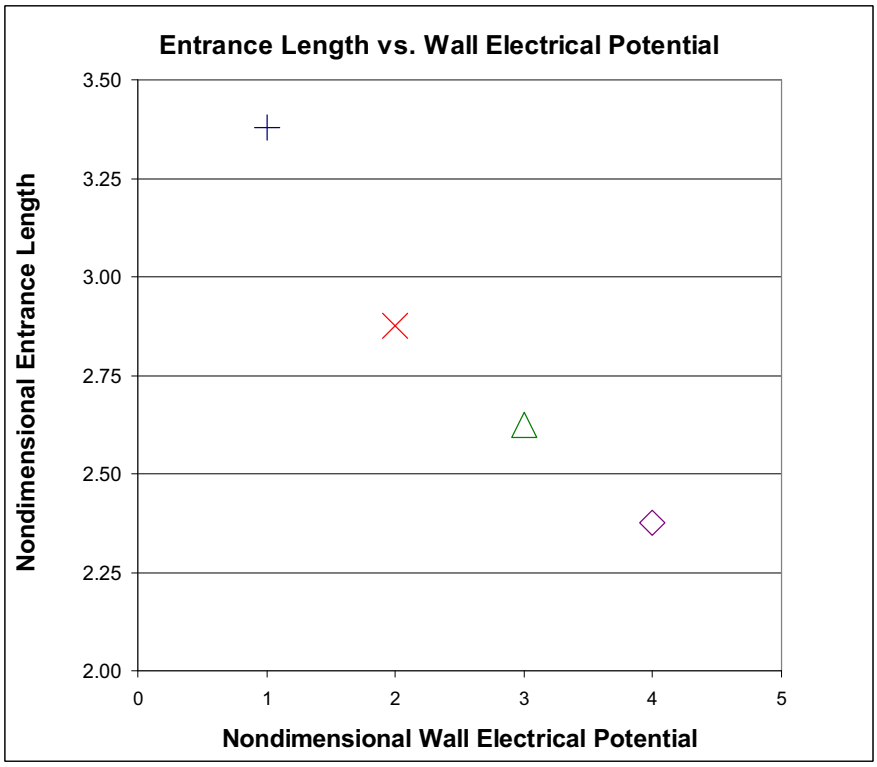

Figure 15: Nondimensional entrance length, L_e vs. nondimensional wall electrical potential, $\overline{\xi}_0$, ($\diamondsuit$:$\overline{\xi}_0$=1, Δ: $\overline{\xi}_0$=2, **x**: $\overline{\xi}_0$=3, +:$\overline{\xi}_0$=4).

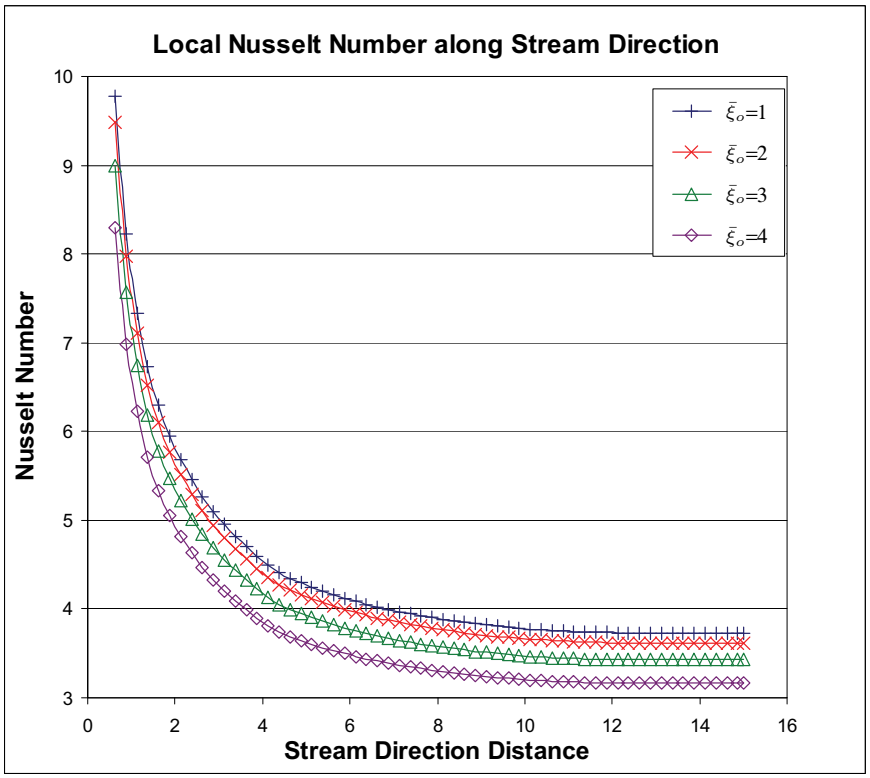

Figure 16: Local Nusselt number along z-direction (streamwise).

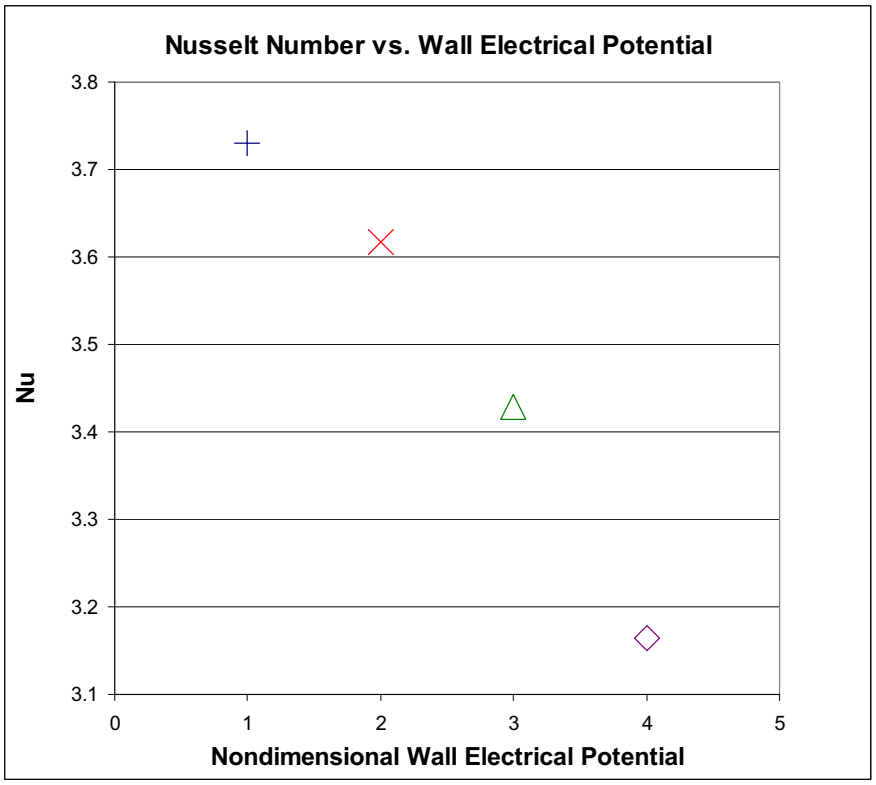

Figure 17: Nusselt number in the fully developed region vs. nondimensional wall electrical potential, $\overline{\xi}_0$ ($\diamondsuit$:$\overline{\xi}_0$=1, Δ: $\overline{\xi}_0$=2, **x**: $\overline{\xi}_0$=3, **+**:$\overline{\xi}_0$=4).

3.3.2 Entrance length, L_e

The relationship between the nondimensional entrance length and wall electrical potential is summarized in Fig. 15. Due to the higher ion concentration, the effective viscosity of the flow is stronger hence the flow fully developed faster and thus shorter developing length is needed; the strong EDL effect will cause a shorter developing length required.

3.3.3 Nusselt number, Nu

Due to the ineffectiveness of heat transfer for the flow field with EDL effect, Fig. 16 illustrates the Nusselt number decreases as the nondimnensional wall electrical potential increases. It is also noted that, near the entrance, the Nusselt number for all $\overline{\xi}_o$ values are almost identical. This reveals that the effect of EDL is significant only at further downstream from the entrance. Fig. 17 suggests that high Nusselt number exists (9 times as compared to the fully developed region) at the entrance of the microchannel which implies that the study of EDL effect on heat transfer effect in the developing region in a 3D microchannel cannot be omitted.

As shown in Fig. 17, *Nu* in the fully developed region increases with smaller wall electrical potential. It shows that the higher wall electrical potential the more significant the EDL effect, thus higher viscous drag force and causes higher heat dissipation and leads to the lower Nusselt number.

4 Conclusion

The important performance of microchannel 3D developing flow such as aspect ratio, *AR*, wall electrical potential, ξ_o, and Schmidt number, *Sc*, at different aspect- ratios (*AR*), Schmidt Number (*Sc*) and Wall Electrical Potential ($\overline{\xi}_o$) is analysed and discussed.

It is found that due to larger relative surface area, the higher the *AR*, the higher fRe and *Nu* values with shorter L_e will be. The effect of *Sc* is not so

significant however the higher the *Sc* value produces the lower fRe. As the $\overline{\xi}_o$ is directly related to the EDL, the higher the $\overline{\xi}_o$ value results the higher fRe and lower L_e values, however higher fRe leads to higher fluid temperature and causes lower *Nu* value.

References

Fu, L.M.; Yang, R.J.; Lee G.B. (2002): Analysis of Geometry Effects on Band Spreading of Microchip Electrophoresis, *Electrophoresis 2002*, vol. 23, pp. 602-612.

Fu, L.M.; Lin, J.Y.; Yang, R.J. (2003) Analysis of electroosmotic flow with step change in zeta potential, *Journal of Colloid and Interface Science*, vol. 258, pp. 266-275

Mala, G.M.; Li, D.; Dale, J.D. (1997): Heat Transfer and Fluid Flow in Microchannels, *Int. J. Heat Mass Transfer*, vol. 40, pp. 3079-3088.

Ng E.Y.K.; Poh S.T. (2002): Modeling of electric double layer effects through pressure-driven microchannel flows, *CMES: Computer Modeling in Engineering & Sciences*, vol. 3, no. 3, pp. 351-365.

Ng, E.Y.K.; Tan, S.T. (2004): Computation of 3D Developing Pressure-driven Liquid Flow in Microchannel with EDL Effect, *Numerical Heat Transfer, Part A: Applications*, vol. 45, no. 10, pp. 1013-1027.

Ng, E.Y.K.; Tan, S.T. (2007): Study of EDL Effect on 3D Developing Flow in Microchannel with Poisson-Boltzmann and Nernst-Planck Models, *International Journal for Numerical Methods in Engineering*, vol. 71, no. 7, pp. 818-836.

Patankar, S.V. (1980): *Numerical Heat Transfer and Fluid Flow*, McGraw-Hill, New York.

Roache, P.J. (1994):Perspective: A method for uniform reporting of grid refinement studies, *ASME Journal of Fluids Engineering*, vol. 116, pp. 405-413.

Shah, R.K.; London A.L. (1978): *Laminar Flow Forced Convection in Ducts, A Source Book for Compact Heat Exchanger Analytical Data*, Academic Press, New York.

Tan S.T.; Ng, E.Y.K. (2003): Numerical Studies of Developing Flow in Microchannel, Int. *J. of Computational Engineering Science, Special Issue on MEMs*, vol. 4, no. 2, pp. 389-392.

Tardu, S. (2004): Analysis of the Electric Double Layer Effect on Microchannel Flow Stability, *Micro scale Thermophysical Engineering*, vol. 8, no. 4, pp. 383-401.

Tuckennan, D.B. (1984): Heat-transfer microstructures for integrated circuits, Ph.D. Diss., Stanford University, USA.

Yang, R.J.; Fu, L.M.; Hwang, C.C. (2001): Electroosmotic entry flow in a microchannel, *Journal of Colloid and Interface Science*, vol. 244, pp. 173-179.

Zhong, Z.; Dai, Y.; Mei, C.C.; Tong, P. (2002): A Micromechanical Theory of Flow in Pulmonary Alveolar Sheet, *CMES: Computer Modeling in Engineering & Sciences*, vol. 3, no. 1, pp. 77-86